

# Coronal heating distribution due to low-frequency wave-driven turbulence

P. Dmitruk<sup>1</sup>, W. H. Matthaeus<sup>1</sup>, L. J. Milano<sup>1</sup>,  
S. Oughton<sup>2</sup>, G. P. Zank<sup>3</sup> and D. J. Mullan<sup>1</sup>

<sup>1</sup>*Bartol Research Institute, University of Delaware, Newark, DE 19716*

<sup>2</sup>*Department of Mathematics, University College London, England*

<sup>3</sup>*Institute of Geophysics and Planetary Physics (IGPP), University of California, Riverside*

pablo@bartol.udel.edu

## ABSTRACT

The heating of the lower solar corona is examined using numerical simulations and theoretical models of magnetohydrodynamic turbulence in open magnetic regions. A turbulent energy cascade to small length scales perpendicular to the mean magnetic field can be sustained by driving with low-frequency Alfvén waves reflected from mean density and magnetic field gradients. This mechanism deposits energy efficiently in the lower corona, and we show that the spatial distribution of the heating is determined by the mean density through the Alfvén speed profile. This provides a robust heating mechanism that can explain observed high coronal temperatures and accounts for the significant heating (per unit volume) distribution below two solar radius needed in models of the origin of the solar wind. The obtained heating per unit mass on the other hand is much more extended indicating that the heating on a per particle basis persists throughout all the lower coronal region considered here.

*Subject headings:* Sun: corona — MHD — turbulence

## 1. Introduction

The mechanism by which the solar corona is heated is a fundamental problem in astrophysics and plasma physics, and one that remains incompletely explained. An acceptable mechanism transports energy to the corona, heating it to temperatures greatly in excess of chromospheric values. This mechanism accelerates the solar wind and establishes the boundary conditions for the entire plasma heliosphere. There are several constraints on an

acceptable coronal heating model. Spectrometers (Kohl et al. 1995; Kohl et al. 1997) show that proton temperatures in polar coronal holes rise to several  $10^6$  K at heliocentric distances of 1.5 to 2 solar radii ( $R_s$ ) and the bulk wind speed reaches 200 km/s. Remote sensing observations (Grall et al. 1996) indicate wind speeds up to 600 km/sec at  $4 R_s$ . Fluid models of the solar wind (Habbal et al. 1995; McKenzie et al. 1995; Evje & Leer 1998) support the conclusion that wind acceleration at such low altitudes requires heating low in the corona. In the fluid models an *ad hoc* heating function  $Q(r)$  is assumed, which represents the energy deposition per unit volume as  $Q \equiv Q_0 \exp\left[-\frac{r-r_0}{L}\right]$ , where  $r$  is heliocentric distance,  $r_0 = R_s \approx 7 \times 10^5$  km,  $L$  is a prescribed dissipation lengthscale, and  $Q_0$  is chosen so that the energy flux has the required value of about  $5 \times 10^5$  erg  $\text{cm}^{-2}\text{s}^{-1}$  (Withbroe & Noyes 1977). Despite the fact that there is no direct observational evidence for the exponential heat function, it has been long known to provide (Holzer & Axford 1970; Kopp & Orrall 1976; Hammer 1982) rapid acceleration of the wind, and with  $L \approx 0.2\text{--}0.5 R_s$  it accounts for many observed features of the corona (McKenzie et al. 1995; Habbal et al. 1995; Axford & McKenzie 1997). Although some possible sources of heating are proposed, in those models there is no physical mechanism for explaining this heating function and, being an *ad hoc* quantity, the exact explicit exponential function expression is perhaps irrelevant and the main point to be remarked is the requirement of strong heating per unit volume in the first solar radius of the corona. Yet other two-fluid (electrons and protons) models (Tu & Marsch 1997; Marsch & Tu 1997) have included some mechanisms for the heating, based on the requirement of high frequency waves launched from the Sun, but those high frequencies (of the order of KHz) waves have yet remained unobserved in the coronal base where the energy is injected. In another previous approach, Hollweg 1986; Hollweg & Johnson 1988; Isenberg 1990 conjectured that waves are launched from the Sun at low frequencies but magnetohydrodynamic (MHD) turbulent-like cascades are assumed to transfer the energy to higher frequencies, where ion cyclotron mechanisms can be invoked to dissipate it. This idea, recently employed by Li et al. 1999 and reviewed by Cranmer 2000 involve phenomenological turbulent rates (being called of the Kolmogorov and Kraichnan type) but two important problems are faced. First, a cascade in wave frequencies is assumed, which implies a turbulent cascade proceeding in the parallel (to the mean field) wavenumber direction and a linear dispersion relation to persist between parallel wavenumber and frequency. MHD simulation studies show on the other hand that in the presence of a strong mean magnetic field, like in the corona, the parallel wavenumber cascade is almost completely suppressed (Shebalin et al. 1983; Oughton et al. 1994; Matthaeus et al. 1998) in favor of the perpendicular cascade. This is precisely the kind of anisotropy which is well documented (Armstrong et al. 1990) for the lower coronal density.

Second, the necessity of counterpropagating fluctuations to sustain the turbulence

(Kraichnan 1965; Dobrowolny et al. 1980) is not considered in the models and a WKB approach is implicitly assumed. In those models, the turbulent cascade was not the central focus of study, but we believe that a useful perspective can be gained into the heating problem by further study of this issue. In this present work, instead of assuming a parallel wave cascade, we describe *ab initio* the conditions under which a strong (perpendicular) turbulent cascade can actually be developed and sustained by low frequency driving at the base. Reflections from density and mean field gradients provide the necessary counterpropagating fluctuations to sustain the turbulence and this effect is fully taken into account in our model. We will employ both direct numerical simulation and turbulent phenomenologies to obtain the heating rate distribution.

We show that the heating distribution profile is related to the coronal background magnetic field and density profile, i.e., the heating and the density profile are not independent quantities. On the one hand, we find that the heating per unit volume is significant mostly within the first solar radius, with a dissipation length scale (defined as the length in which the heating decays by an order of magnitude) of a fraction of solar radius. On the other hand the heating per unit mass varies much less dramatically and is significant through the complete domain. For a complete model, appropriate kinetic processes will need to be identified to absorb the small perpendicular scale cascaded energy. Candidates for small scale damping are plentiful, and include oblique kinetic Alfvén waves, collisionless reconnection and associated heating at current sheets and nonlinear beam instabilities (Leamon et al. 1998). The kinetic physics of heating is beyond the scope of the present paper. The main purpose of this work is to show that a heating distribution emerges naturally from a consistent MHD turbulent cascade driven by low frequency fluctuations at the coronal base. This result may bring us closer to understand the puzzle of coronal heating and the origin of the solar wind.

## 2. Model

Most coronal heating models derive their energy supply from either wave power or quasi-static field line motions, originating in the photosphere or chromosphere. These differ mainly in their characteristic timescales. A general scenario for wave production in open magnetic regions has been proposed (McKenzie et al. 1995) in which activity in the network regions, driven by convective motions, provides a source of upward traveling Alfvén waves. Higher frequency waves are easily transported upward, whereas low-frequency waves experience greater reflection and transmit less readily into the corona (Parker 1965; Heinemann & Olbert 1980; An et al. 1990; Zhou & Matthaeus 1990; Velli 1993). However even in the limit of sharp gradients or discontinuities, there are indications (Hollweg 1981)

that a substantial energy flux can reach the coronal base (Kudoh & Shibata 1999).

Here we examine the following scenario (Matthaeus et al. 1999): MHD-scale ( low-frequency ) fluctuations are excited below the base of the corona, on transverse length scales that are characteristic of the chromospheric network, and propagate upwards along the mean magnetic field  $\mathbf{B}$ . A portion of this wave flux enters the corona. Reflections from large-scale inhomogeneities within the lower corona produce counter-propagating fluctuations (Heinemann & Olbert 1980; Zhou & Matthaeus 1990) a situation that permits strong nonlinear MHD couplings (Dobrowolny et al. 1980). The couplings drive a perpendicular (to  $\mathbf{B}$ ) turbulent cascade, producing small scale reconnection events that couple to kinetic processes at small scales and oblique wavevectors (Leamon et al. 1998).

In our model, we simulate the propagation of low-frequency MHD fluctuations in a medium whose properties are chosen to represent an open magnetic field region (like a polar coronal hole) in the lower corona. We consider a volume section which extends in the radial direction a distance  $L_s$  of order  $2R_s$  above the surface. A sketch of such a region is shown in Fig. 1.

Our goal is to compute the dynamics of transverse fluctuations of magnetic field  $\mathbf{b}$  and velocity  $\mathbf{v}$  as influenced by specified large-scale inhomogeneities (mean magnetic field and density gradients) as well as by local nonlinear couplings. To do this, in a medium where there is a strong mean magnetic field, we use the reduced MHD (RMHD) approximation (Strauss 1976; Montgomery 1982; Zank & Matthaeus 1992). This approach is appropriate for fluctuations in a nearly incompressible plasma, where the plasma beta (ratio of thermal to magnetic pressure) is low (Zank & Matthaeus 1992). We employ the Elsasser variables  $\mathbf{z}_{\pm} = \mathbf{v} \pm \mathbf{b}$  (where the magnetic field is written in units of  $\mathbf{b}/\sqrt{4\pi\rho}$ , with  $\rho$ =density) to represent downward (+) and upward (-) propagating fluctuations. Fluctuations depend on the radial coordinate  $r$ , the transverse spatial coordinates (including an areal expansion factor  $A(r)$ ) and on time  $t$ . Mean quantities like density  $\rho$  and magnetic field  $\mathbf{B}$  are assumed to depend only on  $r$ . Consistency with the RMHD assumptions (Zank & Matthaeus 1992) requires  $\partial_r \ll \nabla_{\perp}$ ,  $V_A \gg z_{\pm}$ , and  $\nabla_{\perp} \cdot \mathbf{z}_{\pm} = 0$ , where  $\mathbf{V}_A = \mathbf{B}/\sqrt{4\pi\rho}$  is the Alfvén speed which gives the propagation velocity of fluctuations in the linear limit.

In the presence of a non-uniform  $V_A$ , the nonlinear RMHD equations can be written (Zhou & Matthaeus 1990) as

$$\begin{aligned} \frac{\partial \mathbf{z}_{-}}{\partial t} + V_A \frac{\partial \mathbf{z}_{-}}{\partial r} &= -R_1 \mathbf{z}_{+} + R_2 \mathbf{z}_{-} - \mathbf{z}_{+} \cdot \nabla_{\perp} \mathbf{z}_{-} + \eta \nabla_{\perp}^2 \mathbf{z}_{-} \\ \frac{\partial \mathbf{z}_{+}}{\partial t} - V_A \frac{\partial \mathbf{z}_{+}}{\partial r} &= R_1 \mathbf{z}_{-} - R_2 \mathbf{z}_{+} - \mathbf{z}_{-} \cdot \nabla_{\perp} \mathbf{z}_{+} + \eta \nabla_{\perp}^2 \mathbf{z}_{+} \end{aligned} \quad (1)$$

where  $\eta$  is the resistivity (assumed equal to the viscosity), and  $R_1(r), R_2(r)$  are specified

reflection rates due to the inhomogeneous  $V_A(r)$ . For a symmetric radial geometry ( $A(r) = r^2$ ),  $B = B_0(r_0/r)^2$  (with  $B_0$  the magnetic field at  $r_0 = R_s$ ), the reflection rates are  $R_1(r) = \frac{1}{2} \frac{dV_A}{dr}$  and  $R_2(r) = \frac{1}{2} \frac{dV_A}{dr} + \frac{V_A}{r}$ . In the case of a general geometry with cross section area  $A(r)$ , where  $A(r) = A_0 B_0/B(r)$ , the reflection rates are  $R_1(r) = \frac{1}{2} \frac{dV_A}{dr}$  and  $R_2(r) = \frac{1}{2} \frac{dV_A}{dr} + \frac{1}{2} \frac{V_A}{A} \frac{dA}{dr}$ . The previous expressions are valid for a section with transverse dimensions small compared to the longitudinal size and close to the polar region in the Sun (dependence of the mean field  $B$  with the latitudinal angle should be assumed to maintain the free divergence condition,  $\nabla \cdot \mathbf{B} = 0$ ).

A Chebyshev-Fourier representation is chosen to solve the equations (1) using a direct numerical simulation of the pseudospectral type. Transverse coordinates are periodic, while non periodic boundary conditions are imposed on the bottom and top sections of the volume. In order to model the input of velocity fluctuations at the base of the coronal domain, we refer to observations of non-thermal velocity amplitudes in the upper transition region of the Sun. These amplitudes are reported to range from 20 to 55 km/sec (Chae et al. 1998; Doyle et al. 1998; Hassler et al. 1990). The system of nonlinear equations (1) is driven by imposing a time dependent oscillatory pattern of velocity and magnetic field at the bottom surface, with a transverse lengthscale corresponding to supergranule diameters of 13-32 Mm at the coronal base (Hagenaar et al. 1997) and the typical inter-network spacing of 30 Mm (Axford & McKenzie 1997). Transverse dimensions of the simulation box are chosen to include about 4 supergranules. In the bottom panel of Fig. 2 the boundary conditions imposed on the form of waves at the bottom of the domain are shown. The top panel of Fig. 2 shows a cross section of the volume above in the coronal simulation (corresponding to one of the simulations to be described below). Numerical resolution of  $128 \times 128 \times 33$  Fourier+Chebyshev grid points are employed in this simulation, for a macroscopic Reynolds number of order 600. The fluctuating fields are highly structured on the transverse directions as shown by concentrations of current density in the form of sheet-like small scale structures.

Driving is at a low frequency of  $f = 0.6/t_A$ , where  $t_A = R_s/V_{A_0}$  is a vertical Alfvén crossing time based on the Alfvén velocity at the base and a distance of a solar radius. This correspond to driving wave periods of the order of 1000 sec.

Open boundary conditions are assumed at the top surface. If reflections were absent, this would lead to a wavetrain of upward propagating fluctuations that would escape continuously from the upper boundary without depositing any energy in the system. The system would dynamically relax toward a maximal cross helicity state (Dobrowolny et al. 1980; Grappin et al. 1983; Ting et al. 1986) in which downward propagating fluctuations vanish and there would be no incompressible MHD nonlinearities and hence no cascade. However,

the first two terms on the right hand sides of Eqs. (1) are associated with gradients of the wave speed, and these lead to partial reflection of the excited waves. This results in a state with both upward and downward type fluctuations and thus, sustained turbulence. We have presented in a previous numerical study (Dmitruk et al. 2001a) the conditions under which an efficient MHD turbulent perpendicular cascade can be sustained; what is required is occurrence of reflections and non-propagating structures (controlled by the type of boundary conditions imposed). The efficiency of this mechanism on dissipating the injected energy has been demonstrated by both phenomenologies (Matthaeus et al. 1999; Dmitruk et al. 2001b) as well as direct numerical simulations (Dmitruk et al. 2001a; Oughton et al. 2001). Efficiencies (ratio of turbulent dissipation rate by the energy injection rate) averaging between 10 and 40 % can be obtained. Even very weak reflections are capable of sustaining the turbulence and provide effective dissipation.

In the next section we obtain the heating distribution profiles resulting from this turbulent state.

### 3. Heating profiles

We performed numerical simulations employing several different mean magnetic field and density radial profiles. The values at the bottom boundary (Axford & McKenzie 1997; Feldman et al. 1997) have been fixed to  $B_0 = 9$  Gauss, and a number density of  $n_0 = 3.2 \times 10^8 \text{ cm}^{-3}$ , which gives an Alfvén speed at the base of 1100 km/s. With the assumed amplitude of fluctuations of the order of 20–55 km/s, this gives an average energy input flux per unit area,  $F_{A_0} \sim \rho_0 V_{A_0} \langle z_-^2 - z_+^2 \rangle$  of order  $5 \times 10^5 \text{ erg cm}^{-2} \text{ s}^{-1}$  corresponding to the Withbroe & Noyes 1977 value. These values have to be taken as order of magnitude quantities but a different choice would not invalidate the general argument we want to present here. In our first simulation we consider a symmetric radial mean magnetic field profile  $B(r) = B_0(R_s/r)^2$ . The mean density follows from the hydrostatic equilibrium approximation (An et al. 1990; Velli 1993; Nakariakov et al. 2000):  $dp/dr = -m_i n g$ , with  $p =$  thermal pressure,  $n =$  number density,  $m_i$  the proton mass and  $g =$  gravity. In an isothermal corona, this equation takes the form  $dn/dr = -\alpha_T n R_s/r^2$  where  $\alpha_T = \mu GM/R_g T R_s$  ( $\mu$  mean molecular weight,  $G$  gravitational constant,  $M$  solar mass,  $R_g$  gas constant and  $T$  temperature). The quantity  $\alpha_T \approx 12$  for the Sun and a fully ionized hydrogen coronal plasma at  $T = 10^6$  K. The number density distribution is then  $n(r) = n_0 \exp[\alpha_T(R_s/r - 1)]$  and the density is  $\rho(r) = m_i n(r)$ . We consider two such density profiles, shown in the top left panel of Fig. 3 with continuous and dotted lines, corresponding to values of  $\alpha_T = 12$  and  $\alpha_T = 6$  (representing a hotter corona). This gives two different density profiles, with the hotter corona having

the shallower profile. The corresponding Alfvén speed profiles  $V_A(r) = B(r)/\sqrt{4\pi\rho(r)}$  are shown on the top right panel of Fig. 3. When the system reaches a statistically steady state the turbulent dissipation rate  $\epsilon$  (equal to the cascade rate) is computed from the fluctuating fields  $\mathbf{z}_-$ ,  $\mathbf{z}_+$  from which the heating per unit volume is obtained as  $Q = \rho\epsilon$ .

This quantity is plotted as a function of  $r$  in the bottom left panel of Fig. 3. It is apparent that the dissipation per unit volume is peaked near the model coronal base. It is important to note that  $Q(r)$  decreases faster for the model with the steeper density profile. The radial distance  $\Delta r$  at which  $Q$  decreases by an order of magnitude with respect to the coronal base value  $Q_0$  is  $0.36R_s$  and  $1.1R_s$  for the two profiles in Fig. 3. This would be the analog of the dissipation length in the ad-hoc exponential heating distribution profiles. The bottom right panel on Fig. 3 shows the heating per unit mass, a useful quantity to consider the heating in a per particle basis. Over our entire domain this quantity maintains a relatively constant value. Extended heating per unit mass fits the apparent requirement of a hot (non adiabatic) solar wind and has also emerged in empirical models of radiation loss and other heating models (Mullan and Cheng 1994; Gibson 1973).

A third simulation has been performed employing a super radial geometry, where the mean magnetic field profile has been taken as

$$B = 1.5 \left[ (f_{max} - 1) \left( \frac{R_s}{r} \right)^{3.5} + \left( \frac{R_s}{r} \right)^2 \right] \text{ Gauss} \quad (2)$$

Profiles of this type have been considered in Hollweg 2000 and similar super expansion profiles have been used by McKenzie et al. 1995; Evje & Leer 1998; Li et al. 1999 in their solar wind models. We have taken  $f_{max} = 6$  which gives a boundary value of  $B_0 = 9$  Gauss. An observationally based number density is assumed in this case (Feldman et al. 1997),

$$n(r) = 3.2 \times 10^8 \left( \frac{R_s}{r} \right)^{15.6} + 2.5 \times 10^6 \left( \frac{R_s}{r} \right)^{3.76} \text{ cm}^{-3} \quad (3)$$

The density profile and resulting Alfvén speed profile are shown in the top panels of Fig. 3 (dashed line). The obtained heating per unit volume and heating per unit mass are shown in the bottom panels of Fig. 3 (dashed line). The result confirms the tendency shown for the earlier cases: this profile, with the fastest decreasing density, also has the fastest decreasing heating per unit volume. The decay length for this case is  $\Delta r = 0.2R_s$ . The heating per unit mass remains at a relatively constant value.

The relevant results to be extracted from these simulations for different Alfvén speed profiles is that the heating per unit volume has significant values only within the first solar radius of the lower corona and that the radial profile of the heating is controlled by the radial

profile of the density. As it will be more clear from the phenomenological analysis that follows in the next section, it is actually through the Alfvén speed profile and its gradient that this behavior is manifested.

Whether the radial profile of the heating per unit volume is exactly exponential or not is, we believe, irrelevant and we conjecture that a steep heating profile, like the ones we obtained here, would work as well to explain the fast acceleration of the solar wind.

Fig. 3 contains the essence of the present results, that a reasonable and efficient heating can be obtained from the MHD perpendicular turbulent cascade driven by low frequency waves injected from the bottom. The properties of this heating are controlled by both the amount of energy injected into the system and the background profiles of magnetic field and mean density. To further illustrate this idea and, in some limiting case, to obtain an analytical expression for the heating profile in the low region of the volume considered here, we present in the following section a phenomenological approach to the previous model Eqs (1).

#### 4. Heating profile from a phenomenological model

A nonlinear phenomenology (Dmitruk et al. 2001b) simplifies the study of the wave-driven RMHD heating model. We modify Eqs. (1) as follows: the independent variables, now designated as  $Z_{\pm}(r)$ , are treated as one dimensional wave amplitudes with the same linear transport terms (LHS and reflection terms) as in Eqs. (1), but with the nonlinear and dissipative terms on the RHS replaced by the nonlinear models  $Z_{\mp}|Z_{\pm}|/2\lambda_{\perp}(r)$ . This model entirely suppresses the transverse structure, with the strength of the nonlinear cascade effects represented through a single correlation lengthscale  $\lambda_{\perp}(r)$ . Previous investigations (Dmitruk et al. 2001b) have shown that this phenomenology portrays many of the same physical effects as wave-driven models based upon the full RMHD equations (Dmitruk et al. 2001a; Oughton et al. 2001). We expect this model to correspond to high Reynolds number fully developed RMHD turbulence since the amplitudes  $Z_{-}$  and  $Z_{+}$  are strongly coupled in the adopted forms for the nonlinear terms. We extracted a heating function  $Q(r)$  from a numerical solution to this phenomenological model, using the same parameters as those employed in the full nonlinear RMHD simulations and assuming a correlation lengthscale  $\lambda_{\perp}(r)$  linearly increasing with radius, with a value at the coronal base set to correspond to the inter-network spacing of 30 Mm. The derived  $Q(r)$  is illustrated in Fig. 4 as the thin line. The direct numerical solution of the previous section is shown as the thick line. This corresponds to the simpler hydrostatic density and  $1/r^2$  mean magnetic field profile (similar results are obtained for the super expansion geometry). Despite some



differences on the far region, where  $dV_A/dr$  approaches 0 and the heating is very low, the agreement is pretty good, considering the extreme simplification involved in the phenomenological treatment. Of course, the phenomenology would not be useful for studies of the turbulent cascades and spectra, but it gives the right order of magnitude for the averaged quantities such as the dissipation (heating), when this quantity is not extremely low. The interesting issue of how the correlation length and the strength of the cascade depend on the external parameters warrants further study comparing the phenomenology with the full non linear direct numerical simulation.

In Fig. 5 we explore the phenomenological heat function  $Q$  obtained by varying the correlation lengthscale at the coronal base, with  $\lambda_\perp = 1$  corresponding to 30 Mm. The limit  $\lambda_\perp \rightarrow 0$  corresponds to stronger local turbulence since the implied eddy turnover time  $\lambda_\perp/z_-$  becomes much smaller than the wave transit time  $R_s/V_A$ . Fig. 5 shows that  $Q$  increases as  $\lambda_\perp \rightarrow 0$ , while maintaining the fast radially decreasing behavior.

In this limit, an analytical asymptotic expression can be obtained. Although limited in its validity, this analysis serves to illustrate better the properties of the heating in this model. We begin by formulating a flux balance equation, based upon Eq.(1). This takes the form  $dF/dr = -A(r)Q$ , where the net upward energy flux  $F = \rho A V_A(Z_-^2 - Z_+^2)$  and  $A$  is the cross section area. Note that in geometrical optics (or “WKB” theory for noninteracting waves) (Jacques 1977) the flux balance formally requires that  $Q \equiv 0$ . When fluctuations are damped,  $Q \neq 0$  (Hollweg 1986). Here the crucial relation that connects the heating to the Alfvén speed profile emerges by identifying  $Q$  with a physically correct turbulent dissipation rate per unit volume at distance  $r$ , namely  $Q = \rho \epsilon$ , where the dissipation rate per unit mass  $\epsilon$  is expressed in the phenomenological model as  $\epsilon \approx (Z_+^2|Z_-| + Z_-^2|Z_+|)/\lambda_\perp$ . We now proceed to form an asymptotic strong turbulence limit as follows. Letting  $\lambda_\perp \rightarrow 0$ , one can conclude (Dmitruk et al. 2001b) that the downward flux is small,  $|Z_+| \ll |Z_-|$ , and that in a steady state this limit is characterized by  $|Z_+|/\lambda_\perp = |dV_A/dr|$ . Thus  $\epsilon \approx Z_-^2|Z_+|/\lambda_\perp$  and we obtain the asymptotic result that the dissipation per unit length can be related to the Alfvén speed profile and the energy flux:  $A Q \approx \rho A Z_-^2|dV_A/dr| \approx V_A^{-1}|dV_A/dr|F$ . Thus, the asymptotic flux balance equation can now be written as  $dF/dr \approx -V_A^{-1}|dV_A/dr|F$ , whose solution is

$$F \approx \begin{cases} F_0 V_{A_0}/V_A & \text{if } r < r_m \\ F_0 (V_{A_0}/V_{A_m})^2 V_A/V_{A_0} & \text{if } r > r_m \end{cases} \quad (4)$$

where  $F_0$  is the net flux at the base and  $r_m$  is the radial distance at which  $V_A$  reaches its maximum value  $V_{A_m}$ .

This allows us finally to obtain an explicit expression for the heating deposition

$$Q(r) \approx \begin{cases} F_{A_0} (A_0/A) |dV_A/dr| (V_{A_0}/V_A^2) & \text{if } r < r_m \\ F_{A_0} (A_0/A) |dV_A/dr| (V_{A_0}/V_{A_m}^2) & \text{if } r > r_m \end{cases} \quad (5)$$

where  $F_{A_0} = F_0/A_0$  is the energy flux per unit area at the base (i.e, the Withbroe & Noyes 1977 value).

For the particular case of the  $A = r^2$  geometry and the isothermal atmosphere used before, with  $r_m \approx 3R_s$ , this relation predicts the top dot dashed curve of Fig. 5. As seen in this figure, the phenomenological solutions for different  $\lambda_\perp$  values approach this asymptotic case as  $\lambda_\perp$  tends to 0. Already for  $\lambda_\perp = 1/10$  the asymptotic solution would be a good approximation. This corresponds to correlation length scales of order 3000 km. Although much less than the typical inter network distances, observations do not rule out correlation scales of this magnitude. Eq. (5) also shows that in this limiting case the value of the heating goes to 0 at points where  $dV_A/dr = 0$ , a limitation which is only apparent at corresponding very low values of  $Q$  in the numerical solution (a similar result applies for the super expansion profile presented before, where the point at which  $dV_A/dr = 0$  is  $r_m \approx 1.6R_s$ ).

For this asymptotic limit, eq. (5) explicitly shows that the spatial distribution of turbulent heating is directly connected to the radial profile of the Alfvén speed and its absolute value depends on the energy input flux. This illustrates the connection already pointed out through the direct numerical simulations results.

## 5. Conclusions

We have presented a model for MHD turbulence driven by low-frequency waves imposed at the lower boundary. We applied this model to an open region in the lower corona, adopting reasonable profiles for magnetic field and density. Both direct numerical simulations and phenomenological studies have been performed and compared. Results show that turbulence can be sustained, due to reflection of upward traveling waves by Alfvén speed gradients, producing a perpendicular turbulent cascade and efficient heating. The energy dissipation per unit volume is significant mostly in the lower part of the model corona with a dissipation length scale of a fraction of solar radius. The obtained heating profile  $Q$  is similar to profiles commonly used in solar wind acceleration models. However the more general result emerges, for strong turbulence, that the heat function  $Q(r)$  should be related to the Alfvén speed profile  $V_A(r)$ . This shows that the heating distribution is determined by the large-scale magnetic field and density profiles. In this way one sees that the scale-height of the heating per unit volume is directly related to the density scale-height, thus explaining the spatial confinement of  $Q$  as a consequence of the rapid density decrease in the lower corona. However, the deposition of heat per unit mass  $Q/\rho$  is much more extended, perhaps well beyond the lower coronal region considered in the present model. These conclusions do not rule out other models, such as direct cyclotron absorption of high-frequency waves

(Axford & McKenzie 1997; Tu & Marsch 1997) but they imply that it is possible to provide the proper kind of heating per unit volume using a low-frequency wave-driven MHD turbulence mechanism.

Research supported by NASA (NAG5-7164, NAG5-8134 SEC Theory Program), NSF (ATM-9713595, ATM-0296113), and UK PPARC (PPA/G/S/1999/00059).

## REFERENCES

- Armstrong, J. W., Coles, W. A., Kojima, M. and Rickett, B. J., ApJ, 358, 685.
- An, C.-H., Suess, S. T., Moore, R. L. and Musielak, Z. E. 1990, ApJ, 350, 309.
- Axford, W. I. and McKenzie, J. F. 1997, in *Cosmic Winds and the Heliosphere*, ed. J. R. Jokipii, C. P. Sonnett & M. S. Giampapa (Tucson: Univ. of Arizona Press), 31.
- Chae, J., Schuhle, U. and Lemaire, P. 1998, ApJ, 505, 957.
- Cranmer, S.R. 2000, ApJ, 532, 1197.
- Dmitruk, P., Matthaeus, W. H., Milano, L. J. and Oughton, S. 2001, Phys. Plasmas, 8, 2377.
- Dmitruk, P., Milano, L. J. and Matthaeus, W. H. 2001, ApJ, 548, 482.
- Dobrowolny, M., Mangeney, A. and Veltri, P. L. 1980, Phys. Rev. Lett., 45, 144.
- Doyle, J. G., Banerjee, D. and Perez, M. E. 1998, Solar Phys, 181, 91.
- Evje, H. O. and Leer, E. 1998, A& A, 329, 735.
- Feldman, W.C., Habbal, S.R., Hoogeveen, G. and Wang, Y.-M. 1997, J. Geophys. Res. 102, 26905.
- Gibson, E.G. 1973 in *The Quiet Sun*, NASA SP-303, Washington, D.C.
- Grall, R. R., Coles, W. A., Klinglesmith, M. T. *et al.* 1996, Nature, 379, 429.
- Grappin, R., Pouquet, A. and Léorat, J. 1983, A& A, 126, 51.
- Habbal, S. R., Esser, R., Guhathakurta, M. and Fisher, R. R. 1995, Geophys. Res. Lett., 22, 1465.
- Hagenaar, H. J., Schrijver, C. J. and Title, A. M. 1997, ApJ, 481, 988.

- Hammer, R. 1982, ApJ, 259, 767.
- Hassler, D. M., Rottman, G. J., Shoub, E. C. and Holzer, T. E. 1990, ApJ, 348, L77.
- Heinemann, M. and Olbert, S. 1980, J. Geophys. Res., 85, 1311.
- Hollweg, J. V. 1981, Solar Phys., 70, 25.
- Hollweg, J. V. 1986, J. Geophys. Res., 91, 4111.
- Hollweg, J. V. and Johnson, W. 1988, J. Geophys. Res., 93, 9547.
- Hollweg, J. V. 2000, J. Geophys. Res., 105, 15699.
- Holzer, T. E. and Axford, W. I. 1970, ARA&A, 8, 31.
- Isenberg, P. A. 1990, J. Geophys. Res., 95, 6437.
- Jacques, S. A. 1977, ApJ, 215, 942.
- Kohl, J. L., Gardner, L. D., Strachan, L., Fisher, R. and Guhathakurta, M. 1995, Space Sci. Rev., 72, 29.
- Kohl, J. L., Noci, G., Antonucci, E. *et al.* 1997, Solar Phys., 175, 613.
- Kopp, R. A. and Orrall, F. Q. 1976, A& A, 53, 364.
- Kraichnan, R.H. 1965, Phys. Fluids, 8, 1385.
- Kudoh, T. and Shibata, K. 1999, ApJ, 514, 493.
- Leamon, R. L., Matthaeus, W. H., Smith, C. W. and Wong, H. K. 1998, ApJ, 507, L181.
- Li, X., Habbal, S. R., Hollweg, J. V. and Esser, R. 1999, J. Geophys. Res., 104, 2521.
- Marsch, E. and Tu, C.-Y. 1997, Astron. Astrophys. 319, L17.
- Matthaeus, W. H., Oughton, S., Gosh, S. and Hossain, M. 1998, Phys. Rev. Lett., 81, 2056.
- Matthaeus, W. H., Zank, G. P. Zank, Oughton, S., Mullan, D. J. and Dmitruk, P. 1999, ApJ, 523, L93.
- McKenzie, J. F., Banaszekiewicz, M. and Axford, W. I. 1995, A& A, 303, L45.
- Montgomery, D. C. 1982, Physica Scripta, T2/1, 83.
- Mullan, D. J. and Cheng, Q. Q. 1994, ApJ, 435, 435.

- Nakariakov, V. M., Offman, L. and Arber, T. D. 2000, *A& A*, 353, 741.
- Oughton, S., Priest, E. R. and Matthaeus, W. H. 1994, *J. Fluid Mech.*, 280, 95.
- Oughton, S., Matthaeus, W. H., Dmitruk, P., Milano, L. J., Zank, G. P. and Mullan, D. J. 2001, *ApJ*, 551, 565.
- Parker, E. N. 1965, *ApJ*142, 1086.
- Shebalin, J. V., Matthaeus, W. H. and Montgomery, D. C. 1983, *J. Plasma Phys.*, 29, 525.
- Strauss, H.R. 1976 *Phys. Fluids*, 19, 134.
- Ting, A. C., Matthaeus, W. H. and Montgomery, D. C. 1986, *Phys. Fluids*, 29, 3261.
- Tu, C. -Y. and Marsch, E. 1997, *Sol. Phys*, 171, 363.
- Velli, M. 1993, *A& A*, 270, 304.
- Withbroe, G. and Noyes, R. W. 1977, *ARA&A*, 15, 363.
- Zank, G. P. and Matthaeus, W. H. 1992, *J. Plasma Phys*, 48, 85.
- Zhou, Y. and Matthaeus, W. H. 1990, *J. Geophys. Res.*, 95, 10 291.

Fig. 1 – Sketch of the coronal region considered in this model

Fig. 2 – In the bottom panel the wave forcing applied at the bottom boundary is illustrated with the imposed transverse fluctuating field  $\mathbf{z}_\perp$  (arrows) overlaying the current density (grayscale). In the top panel a cross section at a fraction  $0.2R_s$  above the base is shown with transverse fluctuating field (arrows) over the current density (grayscale) obtained in the numerical simulation. Note the small scale structure formation.

Fig. 3 – The panel at the top left shows three different number density profiles assumed for the simulations. The continuous and dotted line correspond to the hydrostatic model for different values of the density scale height. The dashed line correspond to an observationally based density (see text). The top right panel is the corresponding Alfvén speed profile, with  $1/r^2$  geometry for the hydrostatic density and super expansion geometry for the observational density. The bottom left panel shows the result of the heating per unit volume from the simulations. The bottom right panel is the heating per unit mass.

Fig. 4 – Comparison between the heating per unit volume obtained with the direct numerical simulation of Eqs.(1) (thick line) and the numerical solution of the phenomenological model (thin line), for the case of an hydrostatic density profile and  $1/r^2$  geometry.

Fig. 5 – Different solutions for the heating per unit volume of the phenomenological model (thin lines) for values of the correlation length  $\lambda_\perp = 1, 0.5, 0.1, 0.02$  (in units of the inter network length) which approach the asymptotic solution when  $\lambda_\perp \rightarrow 0$  (Eq.(5) in the text) shown as the dot dashed line.

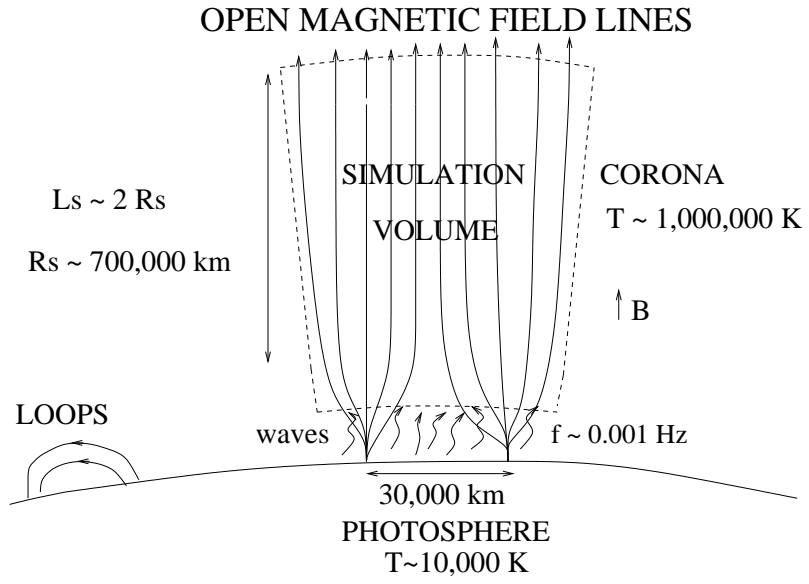
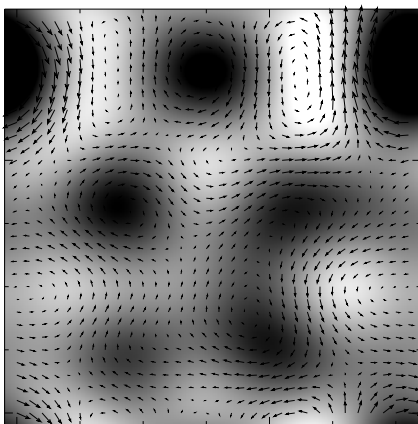
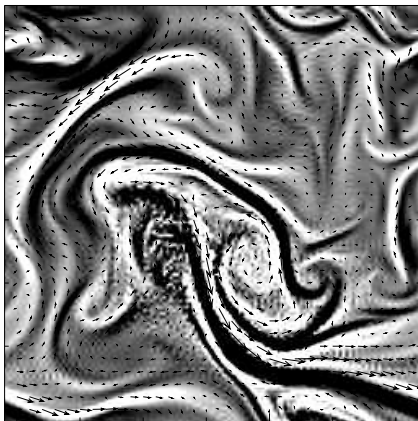


Fig. 1 —





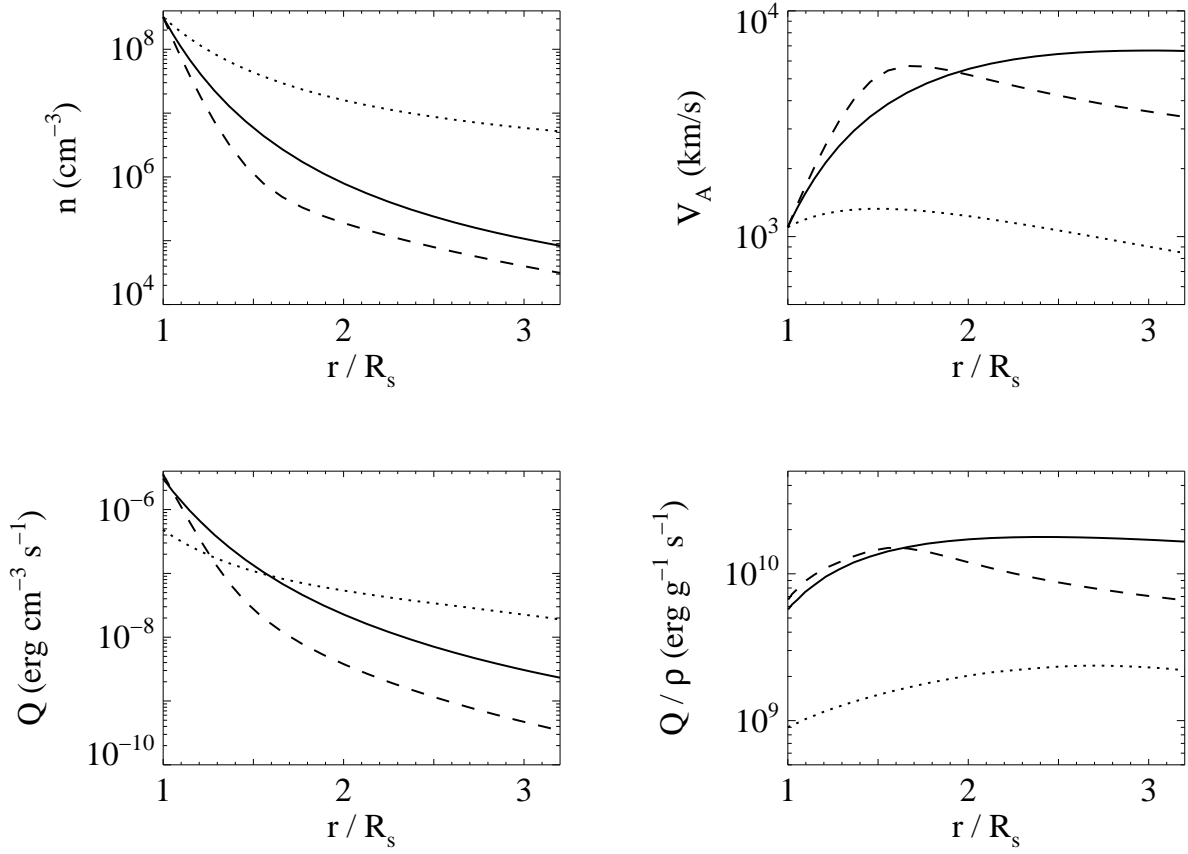


Fig. 3.—

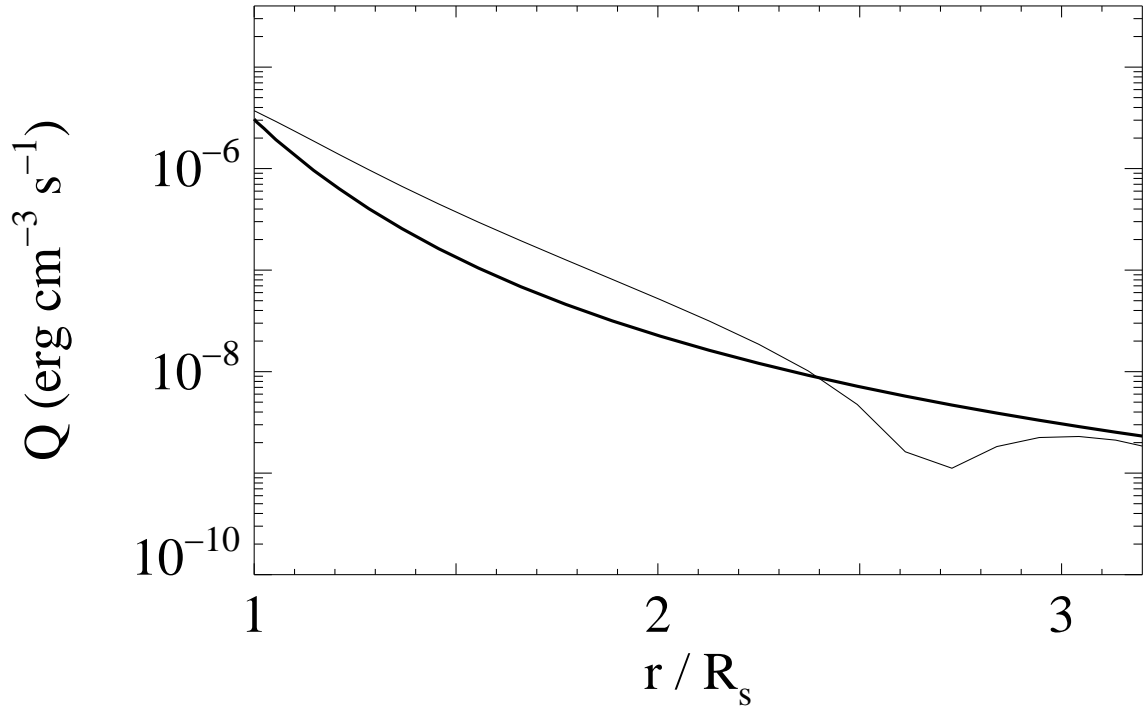


Fig. 4.—

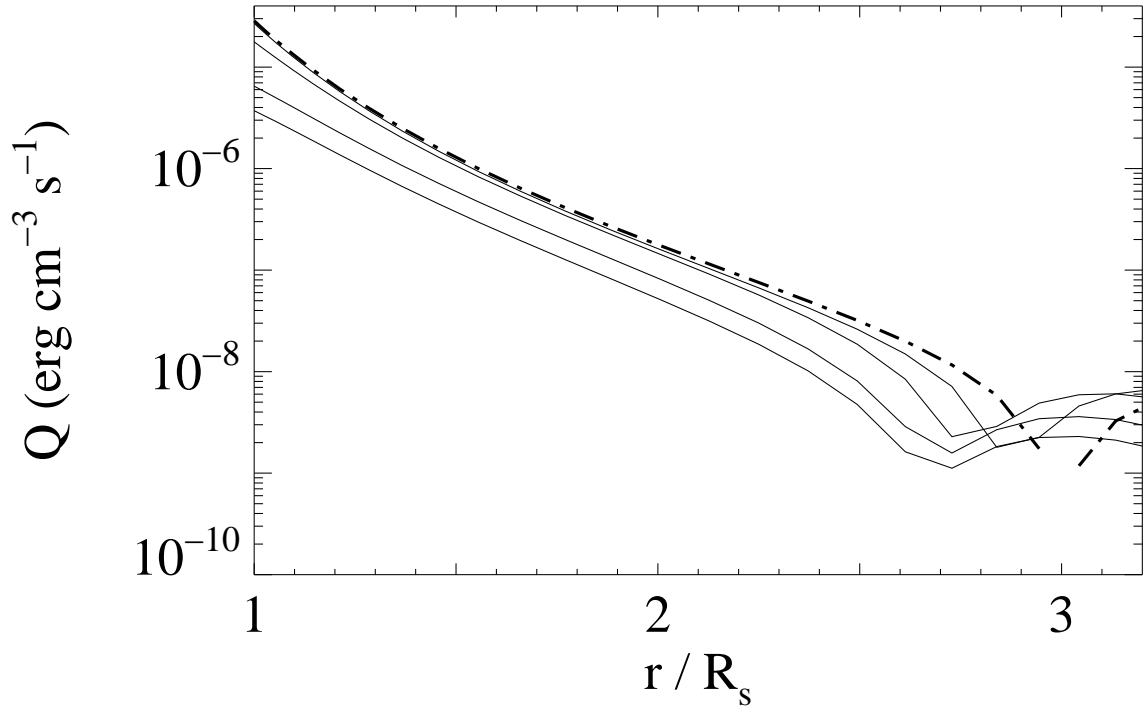


Fig. 5.—